NANO LETTERS

2007
Vol. 7, No. 11
3274−3280

Shape Dependence of Band-Edge Exciton Fine Structure in CdSe Nanocrystals

Qingzhong Zhao,*,† Peter A. Graf,† Wesley B. Jones,† Alberto Franceschetti,‡ Jingbo Li,‡ Lin-Wang Wang,§ and Kwiseon Kim†

Scientific Computing Center, National Renewable Energy Laboratory, 1617 Cole Boulevard, Golden, Colorado 80401, Materials Science Center, National Renewable Energy Laboratory, 1617 Cole Boulevard, Golden, Colorado 80401, and Computational Research Division, Lawrence Berkeley National Laboratory, Berkeley, California 94720

Received June 1, 2007; Revised Manuscript Received August 30, 2007

ABSTRACT

The band-edge exciton fine structure of wurtzite CdSe nanocrystals is investigated by a plane-wave pseudopotential method that includes spin–orbit coupling, screened electron–hole Coulomb interactions, and exchange interactions. Large-scale, systematic simulations have been carried out on quantum dots, nanorods, nanowires, and nanodisks. The size and shape dependence of the exciton fine structure is explored over the whole diameter–length configuration space and is explained by the interplay of quantum confinement, intrinsic crystal-field splitting, and electron–hole exchange interactions. Our results show that the band-edge exciton fine structure of CdSe nanocrystals is determined by the origin of their valence-band single-particle wave functions. Nanocrystals where the valence-band maximum originates from the bulk A band have a "dark" ground-state exciton. Nanocrystals where the valence-band maximum is derived from the bulk B band have a "quasi-bright" ground-state exciton. Thus, the diameter–length configuration map can be divided into two regions, corresponding to dark and quasi-bright ground-state excitons. We find that the dark/quasi-bright ground-state exciton crossover is not only diameter-dependent but also length-dependent, and it is characterized by a curve in the two-parameter space of diameter and length.

Introduction. With the advance in growth methods, semiconductor nanocrystals[1,2] can be synthesized with greater control over their size and shape distribution. For example, the diameter and aspect ratio of CdSe quantum rods can be controlled to within 10%.[3−5] At the same time, more exotic shapes of nanocrystals, such as nanoarrows, nanodrops, nanotetrapods, and nanoribbons, have been synthesized.[6−10] The size dependence of the electronic structure of nanocrystals with specific shapes has been extensively studied over the past two decades. In recent years, experimental and theoretical studies have indicated that the shape dependence can be as important as the size dependence in terms of tuning the electronic and optical properties of the nanocrystals.[11,12] This implies the importance of treating the electronic structure and the optical properties of homogeneous semiconductor nanocrystals as functions of both size and shape. The exciton fine structure, which is sensitive to the nanocrystal size and shape, is particularly interesting not only because it is a test bed to study the interplay of exchange splitting, crystal-field splitting, and quantum confinement, but also because it is critical in designing nanocrystal lasers,[13] nano-biolabels,[14] quantum-dot solar cells, and other nanosized materials.[15,16] In this work, we study in a unified way the band-edge exciton fine structures of CdSe nanocrystals as a function of both size and shape.

The band-edge exciton fine structure was first resolved experimentally in CdSe quantum dots. The combined effects of crystal-field splitting, shape anisotropy, and electron−hole exchange interactions lead to a redshift of the photoluminescence (PL) peak with respect to the first absorption peak (Stokes shift), and to unusually long exciton radiative lifetimes (∼1 μs at 10 K vs 1 ns in bulk).[17] These phenomena have attracted enormous theoretical and experimental interest.[18−22] Using a multiband effective-mass approximation (EMA) model, Efros et al.[20] showed that the lowest-energy exciton, which is 8-fold degenerate in spherically symmetric dots (when neglecting crystal-field splitting), is split into five separate energy levels by crystal-field splitting and electron−hole exchange interactions. The ground-state exciton is optically forbidden. This model[20] describes the size dependence of the Stokes shift and the exciton radiative lifetime in near-spherical quantum dots with good agreement with

* Corresponding author.
† Scientific Computing Center, National Renewable Energy Laboratory.
‡ Materials Science Center, National Renewable Energy Laboratory.
§ Lawrence Berkeley National Laboratory.

10.1021/nl0713070 CCC: $37.00
Published on Web 09/27/2007

experimental data. For nanostructures with shapes far from spherical symmetry, however, the exciton fine structure can be more complicated. In low-temperature, polarization-sensitive PL measurements of single CdSe/ZnS core/shell nanorods, Le Thomas et al.[23] found that the nature (bright or dark) of the ground-state exciton is diameter-dependent. They derived a critical diameter D_{crit} of 7.4 nm, below which the 1D-exciton ground state transforms from a dark state into a bright state. They observed that the PL decay and dynamics of nanorods clearly demonstrate the crossing between bright and dark excitons. Using semiempirical pseudopotential calculations of the electronic states of CdSe quantum rods, Hu et al.[24] showed that the symmetry of the highest occupied states changes as the aspect ratio increases. In spherical quantum dots, the Se $p_{x,y}$ level is higher in energy than the p_z level, whereas, in elongated nanorods, the $p_{x,y}$ level is lower than the p_z level. The calculations of Hu et al.[24] suggest that these two single-particle levels cross when the aspect ratio is 1.3.

To clarify the dark-bright exciton crossover and understand the shape and size dependence of the band-edge exciton fine structure, we investigate CdSe nanocrystals over a large range of shapes: from spherical quantum dots, to nanorods, nanowires, nanodisks, and quantum slabs. Most experimentally grown CdSe nanocrystals are found to have a wurtzite lattice structure because of the stability of the wurtzite lattice over the zincblende lattice. Therefore, in this study, we focus on wurtzite nanocrystals, especially those holding rotational symmetry around the wurtzite *c*-axis. These nanocrystals can be described by only two parameters: the diameter and the length (along the *c*-axis). This simple two-parameter configuration space covers almost all important shapes grown in experiments. We use the term "diameter−length map" to describe the two-parameter configuration space with diameter and length as its *x* and *y* axes. The two-dimensional diameter−length map uniquely defines a nanostructure as a point in the map. Commonly seen nanocrystals, such as quantum dots, nanowires, nanorods, nanodisks, and quantum slabs, can all be described by different points in the map, as shown in Figure 1.

Methods and Simulation Details. CdSe nanocrystals were generated using a "nanostructure generator" software package that is able to generate nanocrystals of arbitrary shape and size. The nanocrystals considered here have the wurtzite lattice structure. The lattice constant a_0 and the internal lattice parameter u are taken from bulk experimental measurements.[25] Surface atoms with more than two dangling bonds are removed, and the remaining surface atoms are passivated by pseudo-hydrogen atoms.[26]

The nanocrystal exciton calculations are divided into two steps. In the first step, we calculate the single-particle states using the semiempirical pseudopotential method (SEPM).[27−29] This approach has been successfully applied in the past to study the optical and electronic properties of semiconductor nanocrystals.[22,24,30−32] In the SEPM method, the single-particle energies $\{\epsilon_i\}$ and wave functions $\{\psi_i(r)\}$ are obtained by solving the Schroedinger equation $\{-(1/2)\nabla^2 + \sum_{n,\alpha} v_\alpha(|r - R_{n,\alpha}|) + V_{SO}\}\psi_i(r) = E_i\psi_i(r)$, where the spin−orbit operator V_{SO} and the screened atomic pseudopotentials $v_\alpha(r)$ are fitted to first-principles bulk potentials and to experimentally determined bulk transition energies, effective masses, and deformation potentials. The single-particle wave functions are expanded in a plane-wave basis set, and the Schroedinger equation is solved using the folded-spectrum method (FSM),[33,34] which allows one to calculate the band-edge eigenstates with a computational effort that scales only linearly with the size of the nanostructure.

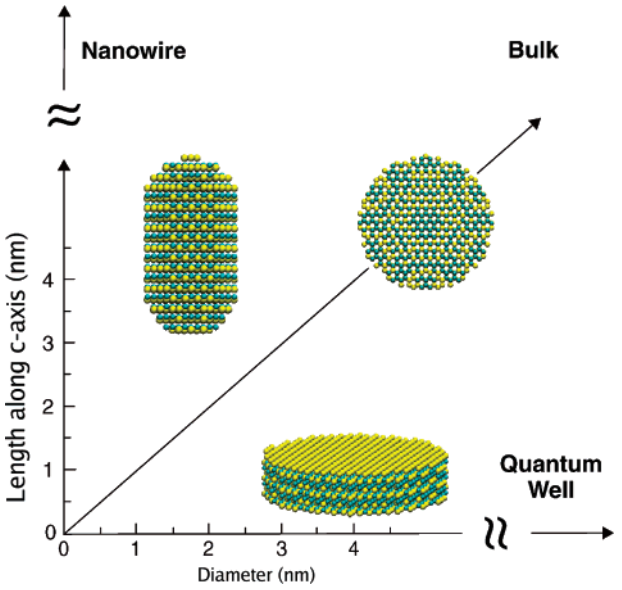

Figure 1. The diameter−length configuration space for wurtzite nanocrystal structures. The length is along the *c*-axis of the wurtzite lattice.

In the second step, we calculate the nanostructure excited states using the configuration interaction (CI) method. NanoPSE,[35,36] a software package that includes the implementation of the SEPM, FSM, and CI methods, is used in our calculations. For the study of band-edge excitons, 8−16 conduction-band and valence-band states are included to ensure the convergence of the ground exciton. The Coulomb and exchange interactions between electron and hole are screened by a position-dependent and size-dependent dielectric constant model.[22] Details of the methodology can be found in refs 22 and 27−34.

In the diameter−length map of Figure 1, the most interesting area is the nanoregion, in which the diameter (D) and length (L) are comparable to or smaller than the bulk exciton diameter (11.2 nm for CdSe). In the limit $L \gg D$, the nanostructures approach nanowires, whereas, for $D \gg L$, the nanostructures approach nanodisks and quantum slabs. In the following sections, we discuss the exciton fine structure of CdSe nanocrystals on the diameter−length map by exploring several series of nanostructures on the diagonal, vertical, and horizontal lines of the diameter−length map. These nanostructures not only illustrate the size and shape dependence of excitons, but also correspond to different controllable growth conditions for spherical dots, nanorods, and nanodisks.

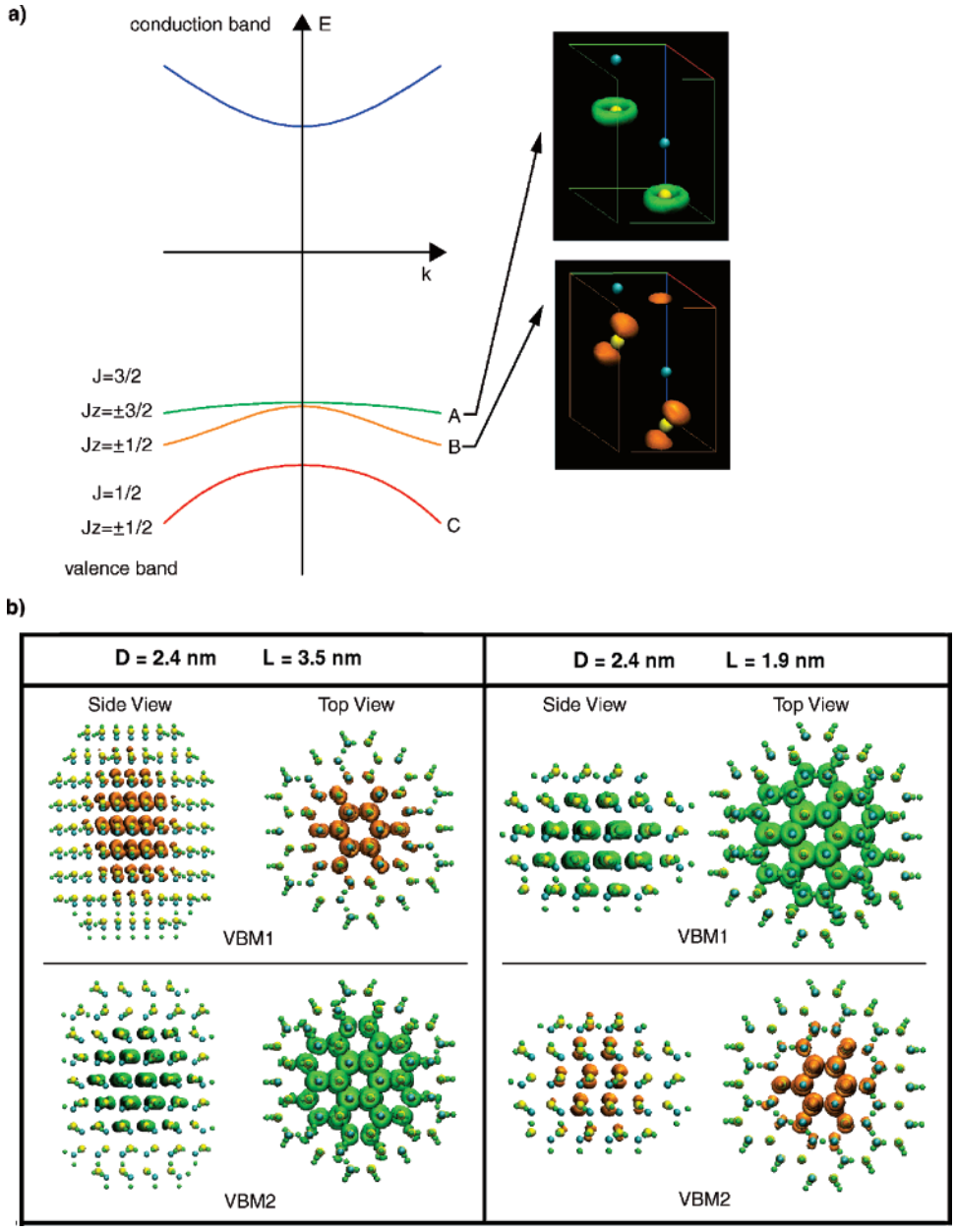

Figure 2. (a) Calculated band structure of bulk CdSe in the wurtzite lattice structure. The wave function amplitude isosurfaces of the two topmost valence-band states are shown on the right-hand side. Note that the A-band and B-band states have very different wave function amplitudes. (b) Wave function amplitude of the two topmost valence-band states (VBM1 and VBM2) in two nanocrystals with the same diameter but different length. The nanorod on the left-hand side has a "quasi-bright" ground-state exciton derived from the bulk B band, whereas the oblate nanocrystal on the right-hand side has a dark ground-state exciton originating from the bulk A band. Note that the B-band wave function amplitude is distributed mainly along the *c*-axis, whereas the A-band wave function amplitude is distributed perpendicular to the *c*-axis.

Band-Edge Exciton Fine Structure of CdSe Nanocrystals. In bulk wurtzite CdSe, the states at the top of the valence band originate from the 4p orbitals of selenium. Wurtzite CdSe has a direct band gap of 1.732 eV at the Γ point. Because of spin−orbit coupling and crystal-field splitting, the top of the valence band splits into three sub-bands, conventionally named the A, B, and C bands (corresponding to the heavy hole, light hole, and split-off bands of zincblende CdSe, respectively). Because the spin−orbit splitting energy (∼418 meV) is much larger than the crystal-field splitting energy (∼25 meV), the C band is located well below the top of the valence band, and only the A and B bands play a role in determining the band-edge exciton fine structure. Therefore, the inclusion of spin−orbit coupling in the calculations is critical to obtain the correct band structure of CdSe. The A band has an angular momentum projection of ±3/2 along the wurtzite *c*-axis, and it originates mainly from the Se $4p_{x,y}$ atomic orbitals. The B band has an angular momentum projection of ±1/2, and originates primarily from the Se $4p_z$ atomic orbitals. Figure 2a shows the wave function amplitude of the A and B bands of bulk CdSe at the Γ point. The A and B bands have very different wave function

amplitudes. The A-band wave function has a donut-shaped amplitude perpendicular to the *c*-axis, whereas the B-band wave function has mostly p_z orbital character along the *c*-axis.

In CdSe nanocrystals, the highest occupied state derives from either the A band or the B band of bulk CdSe, depending on the combined effects of crystal-field splitting and quantum confinement. Figure 2b shows the wave function amplitude of the two top valence-band states of two CdSe nanocrystals of different shape. The highest hole state of the elongated nanorod on the left-hand side of Figure 2b originates from the B band, whereas the highest hole state of the oblate nanodisk on the right-hand side of Figure 2b originates from the A band.

Electron−hole exchange interactions split the 4-fold degenerate A-band exciton into $E^A_{\pm 2}$ and $E^A_{\pm 1}$, and the 4-fold degenerate B-band exciton into E^L_0, $E^B_{\pm 1}$, and E^U_0 (see refs 20 and 22 for detailed definitions of these energy levels). Transitions from the ground state to the $E^A_{\pm 2}$ and E^L_0 exciton states are optically forbidden (dark), whereas transitions to the $E^A_{\pm 1}$, $E^B_{\pm 1}$, and E^U_0 exciton states are optically allowed (bright). The lowest-energy exciton state is $E^A_{\pm 2}$ or E^L_0, depending on the shape and size of the nanocrystal. The splitting between E^L_0 and the next bright exciton states ($E^B_{\pm 1}$) is very small compared to the splitting between $E^A_{\pm 2}$ and $E^A_{\pm 1}$.[37] For example, we find that, in the case of a nanorod 2.4 nm in diameter and with an aspect ratio of 3.2 (see Figure 3a), the splitting between E^L_0 and $E^B_{\pm 1}$ is 1.8 meV, whereas the splitting between $E^A_{\pm 2}$ and $E^A_{\pm 1}$ is 15.7 meV. Thus, CdSe nanocrystals where E^L_0 is the lowest-energy exciton state emit light efficiently, even at very low temperatures,[23] because the bright exciton states $E^B_{\pm 1}$ and E^U_0 are thermally populated. Thus, we will refer to the E^L_0 exciton as a "quasi-bright" exciton. On the other hand, CdSe nanocrystals where $E^A_{\pm 2}$ is the lowest-energy exciton state do not emit light efficiently at low temperatures, so we will refer to the $E^A_{\pm 2}$ exciton states as "dark" excitons.

Results. We have calculated the exciton fine structure of several series of nanostructures covering the nanoregion in the diameter−length configuration map. Along the vertical lines of the diameter−length map, we choose nanostructures with fixed diameters of 1.6, 2.4, 3.2, 3.9, and 4.6 nm, and length ranging from 1.0 to 10 nm. Along the horizontal lines, we choose nanostructures with height/lengths of 1.5, 2.0, and 7.0 nm. These structures include nanodisks, nearly spherical quantum dots, and nanorods. In the case of spherical quantum dots, our calculated exciton fine structure agrees very well with previous multiband EMA[20] and SEPM[22] calculations. Therefore, in the following, we concentrate on non-spherical nanocrystal shapes.

A. Nanorods. Figure 3a shows the exciton fine structure of a series of nanocrystals with the same diameter (2.4 nm) and different length, corresponding to a vertical data line in the diameter−length map of Figure 1. These nanostructures can be grown experimentally by diameter-controlled synthesis. As shown at the top of Figure 3a, the nanostructure shape changes from nanodisk to quantum dot and eventually to nanorod as the length increases. Figure 3b shows the exciton splitting energies of a series of nanocrystals with similar lengths but different diameters, corresponding to a horizontal line in the diameter−length map of Figure 1. In Figure 3b, the first rod on the right-hand side is the longest rod in Figure 3a. In both panels a and b in Figure 3, the exciton energies are referenced from the bright $E^A_{\pm 1}$ excitons, as commonly used in fine-structure studies. This is because the bright exciton energy is a well-defined quantity in both experiments and simulations. As our CI calculations indicate, the eight lowest-energy exciton states originate from the lowest-energy electron level and the two highest-energy hole levels. The highest-energy hole level in the nanodisk and quantum dot of Figure 3a are derived from the bulk A band. The optically forbidden $E^A_{\pm 2}$ exciton states are well separated from the optically allowed $E^A_{\pm 1}$ states; thus, the ground-state excitons of these nanostructures are dark. For the three nanorods shown in Figure 3a, however, the highest-energy hole level originates from the bulk B band. As shown

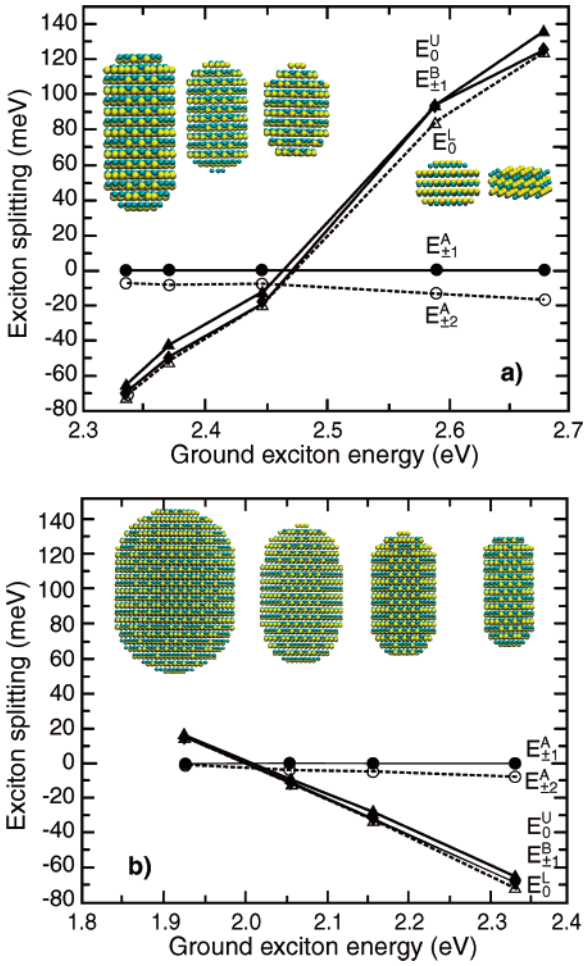

Figure 3. Band-edge exciton fine structure of different CdSe nanocrystals. The exciton energies are shown with respect to the $E^A_{\pm 1}$ state. Bright (dark) exciton states are plotted with solid (dotted) lines. The nanocrystal geometries shown in the upper part of the figure correspond to the data points below them. (a) CdSe nanocrystals with the same diameter (2.4 nm) but different length. (b) CdSe nanocrystals with similar length but different diameter. These two series of nanocrystals show dark/bright exciton crossing. Note the nearly linear trend of the fine-structure splittings with exciton energy.

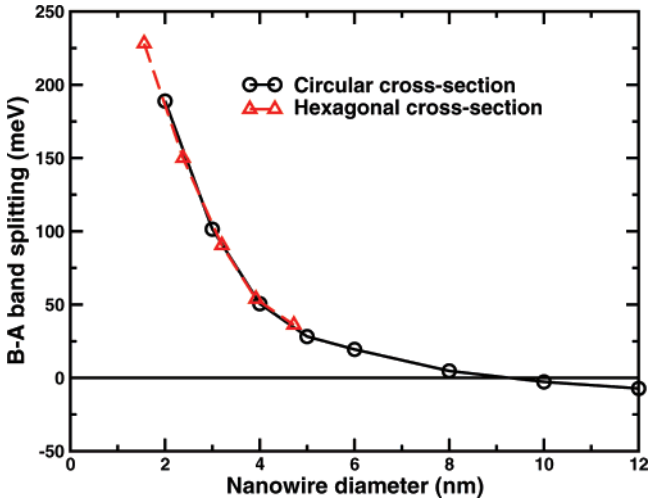

Figure 4. The splitting between the B-band and A-band single-particle hole states is shown as a function of the nanowire diameter. The A/B crossover occurs for $D \sim 9$ nm. Nanowires with circular and hexagonal cross-sections share the same trend.

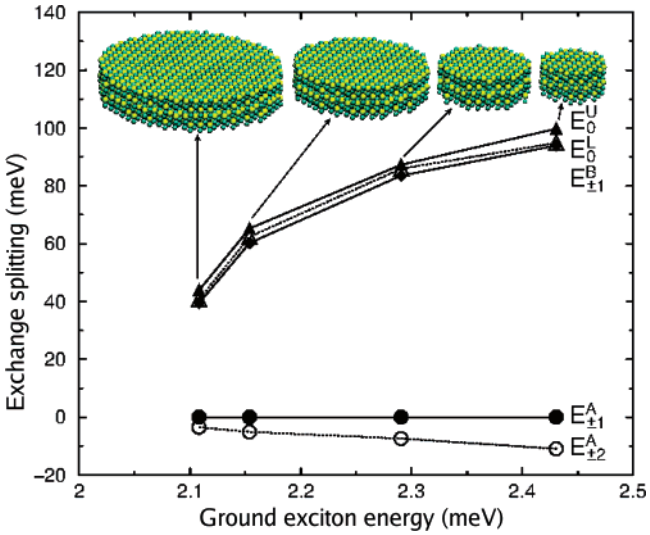

Figure 5. Exciton fine structure of CdSe nanodisks as a function of the ground-state exciton energy. The nanodisks have the same thickness (1.5 nm). Bright (dark) excitons are plotted with solid (dotted) lines. All exciton energy levels are referenced from state $E^{A}_{\pm 1}$.

in Figure 3a, the splitting between the optically forbidden E^{L}_{0} state and the optically allowed $E^{B}_{\pm 1}$ states is very small; thus, the ground-state excitons of these nanostructures are "quasi-bright."

The dark/bright nature of the ground-state exciton is determined by the highest hole state, which, in turn, is controlled by the nanocrystal shape. In nearly spherical or disk-like nanostructures, the crystal-field splitting and strong quantum-confinement effects keep the A-band hole states well above the B-band hole states. In elongated nanorods, however, the increased length along the *c*-axis confines the A-band states more than the B-band states, because the B-band states have charge distribution along the nanorod axis (Figure 2c). Thus, the character of the ground-state exciton switches from dark to quasi-bright as the shape of the CdSe nanocrystal becomes more elongated (Figure 3a). This dark/quasi-bright exciton crossover can also be observed in nanostructures on the horizontal lines of the diameter−length map. In Figure 3b, from right to left, with increasing diameter, the B-band hole state eventually becomes lower than the A-band hole state, so the ground-state exciton becomes dark as the diameter increases.

In both panels a and b of Figure 3, the fine-structure splittings scale approximately linearly with the ground-state exciton energy, although the energy spacings between individual exciton levels are not even, especially for the nanocrystals of Figure 3a.

B. Nanowires. In one-dimensional nanowires, the critical diameter for the dark/quasi-bright exciton transition is determined by the crossover between the A-band and B-band states. The energy difference between the single-particle A- and B-band states is plotted in Figure 4 as a function of the nanowire diameter. The B-band state is higher in energy than the A-band state if the wire diameter is smaller than 9 nm. This critical diameter agrees reasonably well with the experimental value of 7.4 nm,[23] considering that the nanorods measured in experiments (aspect ratio = 10) tend to underestimate the critical diameter, and that there are some differences between CdSe/ZnS core/shell nanorods measured in experiments and the ideally passivated CdSe nanocrystals used in our simulations. Because transmission electron microscope images indicate that CdSe nanocrystals tend to be faceted, it is relevant to understand how the electronic structure changes from faceted structures to non-faceted ones. In Figure 4, non-faceted nanowires with circular cross-sections (open circles) are compared with faceted nanowires with hexagonal cross-sections (open triangles). As far as the A/B-band splitting is concerned, there is no significant difference between cylindrical and hexagonal nanowires.

C. Nanodisks. We explore the nanodisk region by scanning horizontal lines in the diameter−length map. The nanodisk diameter is much larger than its length (height), which leads to reduced quantum confinement of the A band. As expected, the ground-state exciton of nanodisks has strong A-band character, just like spherical quantum dots. Therefore, nanodisks always have dark ground-state excitons. However, the order of the B-band-derived exciton levels is different from that of spherical dots. We find $E^{B}_{\pm 1} < E^{L}_{0} < E^{U}_{0}$, as shown in Figure 5.

Discussion and Conclusions. From the above analysis of the band-edge exciton fine structure of CdSe nanocrystals of different shapes, it is straightforward to draw a "phase diagram" of the dark/bright character of the ground-state exciton as a function of the nanocrystal length and diameter. Figure 6 shows that the diameter−length map can be divided into two continuous regions that correspond to dark and quasi-bright ground-state excitons. Nanocrystals in the upper-left, "quasi-bright" region have a B-band-derived highest hole state, whereas nanocrystals in the lower-right, "dark" region have an A-band-derived highest hole state. As Figure 6 shows, the dark/quasi-bright exciton crossover depends on both the length and diameter of the nanocrystal.

For small-diameter nanocrystals ($D < 4$ nm), the crossover aspect ratio is around 1.3, as in Hu's calculation.[24] For larger-

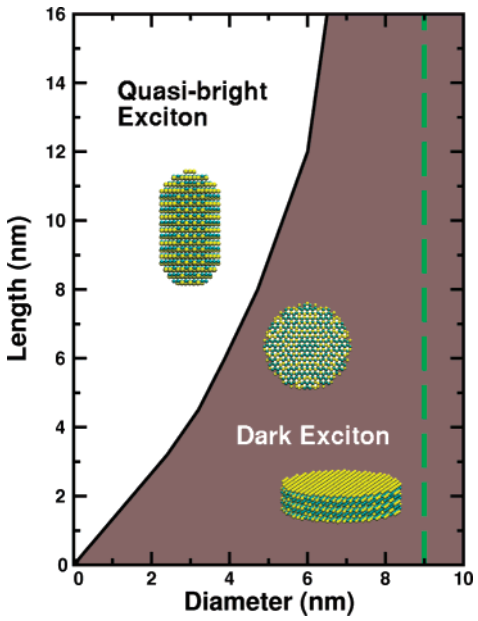

Figure 6. Dark/quasi-bright ground-state exciton map in the diameter−length configuration space. The green dashed line shows the critical diameter ($D_{crit} \sim 9$ nm). The ground-state exciton is dark for structures with diameter $D > D_{crit}$.

diameter nanocrystals ($D \sim 6$ nm), the crossover aspect ratio increases to 2. The crossover aspect ratio was assumed to be diameter-independent in Hu's article,[24] whereas it was considered to depend only on the critical diameter in Le Thomas' study.[23] Both of their conclusions are valid only in the regions of their studied structures. For example, Hu et al.[24] studied nanorods with small diameter; Le Thomas et al.[23] measured nanorods with relatively large aspect ratios (∼10) and large diameters.

One of the most important properties of CdSe nanocrystals is their high fluorescence efficiency, which makes them ideal candidates for applications such as biological imaging, labeling, and sensing.[38] Thus, it is interesting to consider how the dark/bright character of the exciton ground state affects the emission properties of CdSe nanocrystals. Well-passivated CdSe nanocrystals exhibit high fluorescence efficiency because they lack effective nonradiative decay channels. As long as the radiative lifetime is shorter than the nonradiative lifetime, the nanocrystals will emit light efficiently. We have calculated the radiative lifetime of the CdSe nanocrystals in the diameter/length map of Figure 6. We find that, for example, the room-temperature lifetime of the $D = 2.4$ nm, $L = 6.4$ nm nanocrystal (quasi-bright exciton ground state) is 10.3 ns, while the lifetime of the $D = 6$ nm, $L = 6$ nm spherical dot (dark exciton ground state) is 22.8 ns. Therefore, our calculations suggest that CdSe nanocrystals of different size and shape emit light efficiently at room temperature.

In summary, we have studied the band-edge exciton fine structure of CdSe nanocrystals over a wide range of shapes and sizes. Our atomistic pseudopotential calculations allow us to identify two classes of nanocrystal shapes with very different optical properties: (i) Nanorods with diameters smaller than 9 nm and large aspect ratios have a dark ground-state exciton (E_0^L), followed by three bright exciton states ($E_{\pm1}^B$, E_0^U). Because the bright excitons are very close in energy to the dark excitons, the nanocrystal is "quasi-bright." (ii) For all other nanostructures in the diameter−length map, including spherical quantum dots, nanodisks, and nanorods with relatively small aspect ratios or large diameters (≥9 nm), the ground-state exciton is the doubly degenerate dark state $E_{\pm2}^A$, followed by two $E_{\pm1}^A$ bright states. These nanocrystals are "dark." The ordering and splitting of band-edge excitons are explained by the interplay of quantum-confinement, crystal-field splitting, Coulomb interaction and exchange interactions. The systematic study of the exciton fine structure gives a complete picture of the size and shape dependence of band-edge excitons within the two-parameter configuration space examined here. The resulting dark/quasi-bright "phase diagram" (Figure 6) provides guidelines for designing novel nanomaterials.

Acknowledgment. This work is supported by the U.S. DOE-SC-ASCR-Mathematical, Information and Computational Sciences program under the Lab03-17 Theory Modeling in Nanoscience initiative under Contract No. DE-AC36-99GO10337, and for LBNL under Contract No. DE-AC03-76SF00098. We are grateful to NREL-SCC and NERSC for computing facilities and support.

References

(1) Alivisatos, A. P. *Science* **1996**, *271*, 933−937.
(2) Yu, H.; Li, J.; Loomis, R. A.; Gibbons, P. C.; Wang, L. W.; Buhro, W. E. *J. Am. Chem. Soc.* **2003**, *125*, 16168−16169.
(3) Peng, X.; Manna, L.; Yang, W. D.; Wickham, J.; Scher, E.; Kadavanich, A.; Alivisatos, A. P. *Nature* **2000**, *404*, 59−61.
(4) Qu, L.; Peng, Z. A.; Peng, X. *Nano Lett.* **2001**, *1*, 333−337.
(5) Li, L. S.; Hu, J.; Yang, W. D.; Alivisatos, A. P. *Nano Lett.* **2001**, *1*, 349−351.
(6) Peng, Z. A.; Peng, X. *J. Am. Chem. Soc.* **2002**, *124*, 3343−3353.
(7) Manna, L.; Scher, E.; Alivisatos, A. P. *J. Am. Chem. Soc.* **2000**, *122*, 12700−12706.
(8) Manna, L.; Milliron, D.; Meisel, A.; Scher, E.; Alivisatos, A. P. *Nat. Mater.* **2003**, *2*, 382−385.
(9) Milliron, D. J.; Hughes, S. M.; Cui, Y.; Manna, L.; Li, J.; Wang, L. W.; Alivisatos, A. P. *Nature* **2004**, *430*, 190−195.
(10) Yin, Y.; Alivisatos, A. P. *Nature* **2005**, *437*, 664−670.
(11) Li, J.; Wang, L. W. *Nano Lett.* **2003**, *3*, 1357−1363.
(12) Buhro, W. E.; Colvin, V. L. *Nat. Mater.* **2003**, *2*, 138−139.
(13) Klimov, V. I.; Mikhailovsky, A. A.; Xu, S.; Malko, A.; Hollingsworth, J. A.; Leatherdale, C. A.; Eisler, H.-J.; Bawendi, M. G. *Science* **2000**, *290*, 314−317.
(14) Bruchez, M.; Moronne, M.; Gin, P.; Weiss, S.; Alivisatos, A. P. *Science* **1998**, *281*, 2013−2016.
(15) Huynh, W. U.; Dittmer, J. J.; Alivisatos, A. P. *Science* **2002**, *295*, 2425−2427.
(16) (a) Nozik, A. J. *Physica E (Amsterdam)* **2002**, *14*, 115−120. (b) Schaller, R. D.; Klimov, V. I. *Phys. Rev. Lett.* **2004**, *92*, 186601. (c) Schaller, R. D.; Agranovich, V. M.; Klimov, V. I. *Nat. Phys.* **2005**, *1*, 189−194.
(17) Bawendi, M. G.; Wilson, W. L.; Rothberg, L.; Carroll, P. J.; Jedju, T. M.; Steigerwald, M. L.; Brus, L. E. *Phys. Rev. Lett.* **1990**, *65*, 1623−1626.
(18) O'Neil, M.; Marohn, J.; McLendon, G. *J. Phys. Chem.* **1990**, *94*, 4356−4363; Hasselbarth, A.; Eychmuller, A.; Weller, H. *Chem. Phys. Lett.* **1993**, *203*, 271−276.
(19) Norris, D. J.; Efros, Al. L.; Rosen, M.; Bawendi, M. G. *Phys. Rev. B* **1996**, *53*, 16347−16354.
(20) Efros, Al. L.; Rosen, M.; Kuno, M.; Nirmal, M.; Norris, D. J.; Bawendi, M. *Phys. Rev. B* **1996**, *54*, 4843−4856.
(21) Leung, K.; Pokrant, S.; Whaley, K. B. *Phys. Rev. B* **1998**, *57*, 12291−12301.
(22) Franceschetti, A.; Fu, H.; Wang, L. W.; Zunger, A. *Phys. Rev. B* **1999**, *60*, 1819−1829.

(23) Le Thomas, N.; Herz, E.; Schops, O.; Woggon, U. *Phys. Rev. Lett.* **2005**, *94*, 016803-1−016803-4.
(24) Hu, J.; Wang, L. W.; Li, L. S.; Yang, W. D.; Alivisatos, A. P. *J. Phys. Chem. B* **2002**, *106*, 2447−2452.
(25) Madulung, O., Ed. *Landolt-Börnstein New Series, Group III*; Springer-Verlag: Berlin, 1982; Vol. 17b, pp 202−224.
(26) Graf, P. A.; Kim, K.; Jones, W. B.; Wang, L. W. *J. Comput. Phys.* **2007**, *224*, 824−835.
(27) Wang, L. W.; Zunger, A. *Phys. Rev. Lett.* **1994**, *73*, 1039−1042.
(28) Wang, L. W.; Zunger, A. *Phys. Rev. B* **1996**, *53*, 9579−9582.
(29) Wang, L. W.; Zunger, A. *Phys. Rev. B* **1995**, *51*, 17398−17416.
(30) Li, J.; Wang, L. W. *Nano Lett.* **2004**, *4*, 29−33.
(31) Wang, L. W.; Califano, M.; Zunger, A.; Franceschetti, A. *Phys. Rev. Lett.* **2003**, *91*, 056404-1−056404-4.
(32) Franceschetti, A.; Wang, L. W.; Bester, G.; Zunger, A. *Nano Lett.* **2006**, *6*, 1069−1074.
(33) Wang, L. W.; Zunger, A. *J. Chem. Phys.* **1994**, *100*, 2394−2397.
(34) Wang, L. W.; Zunger, A. *J. Phys. Chem. B* **1998**, *102*, 6449−6454.
(35) Jones, W. B.; Bester, G.; Canning, A.; Franceschetti, A.; Graf, P. A.; Kim, K.; Langou, J.; Wang, L. W.; Dongarra, J.; Zunger, A. *J. Phys.: Conf. Ser.* **2005**, *16*, 277−282.
(36) Zunger, A.; Franceschetti, A.; Bester, G.; Jones, W. B.; Kim, K.; Graf, P. A.; Wang, L. W.; Canning, A.; Marques, O.; Voemel, C.; Dongarra, J.; Langou, J.; Tomov, S. *J. Phys.: Conf. Ser.* **2006**, *46*, 292−298.
(37) From multiband EMA exciton energy levels, $|E^{A}_{\pm 2} - E^{A}_{\pm 1}| = 2\Delta_x + 1/2\Delta_{CF} - \sqrt{[(2\Delta_x - \Delta_{CF})^2]/4 + 3\Delta_x^2}$, and $|E^{L}_{0} - E^{B}_{\pm 1}| = 2\Delta_x - 1/2\Delta_{CF} + \sqrt{[(2\Delta_x - \Delta_{CF})^2]/4 + 3\Delta_x^2}$. Because crystal-field splitting is normally much larger than exchange splitting ($\Delta_{CF} \gg \Delta_x$), $\sqrt{[(2\Delta_x - \Delta_{CF})^2]/4 + 3\Delta_x^2} = 1/2\Delta_{CF}[1 - 4(\Delta_x/\Delta_{CF}) + 16(\Delta_x/\Delta_{CF})^2]^{1/2} \approx 1/2\Delta_{CF}(1 - 2(\Delta_x/\Delta_{CF})) = 1/2\Delta_{CF} - \Delta_x$. Therefore, $|E^{A}_{\pm 2} - E^{A}_{\pm 1}| \approx 3\Delta_x$, and $|E^{L}_{0} - E^{B}_{\pm 1}| \approx \Delta_x$. The exchange splitting between A-band dark/bright excitons is about 3 times that of the splitting between B-band dark/bright excitons.
(38) Medintz, I. L.; Uyeda, H. T.; Goldman, E. R.; Mattoussi, H. *Nat. Mater.* **2005**, *4*, 435−446.

NL0713070